Journal of Power Sources 551 (2022) 232221

Contents lists available at ScienceDirect

Journal of Power Sources

journal homepage: www.elsevier.com/locate/jpowsour

Constrained hydrocarbon-based ionomers in porous Poly (tetrafluoroethylene) supports for enhanced durability of polymer electrolyte membrane fuel cells and water electrolyzers

Seung Jae Hong [a,b,1], Hwan Yeop Jung [a,1], Sang Jun Yoon [a], Keun-Hwan Oh [a], Seong-Geun Oh [b], Young Taik Hong [a], Duk Man Yu [a,**], Soonyong So [a,*]

[a] Energy Materials Research Center, Korea Research Institute of Chemical Technology, 141 Gajeong-ro, Yuseong-gu, Daejeon, 34114, South Korea
[b] Department of Chemical Engineering, Hanyang University, 222 Wangsimni-ro, Seongdong-gu, Seoul, 04763, South Korea

HIGHLIGHTS

- Three-layered SPAES reinforced membranes were prepared.
- The reinforcement stress was around 28 MPa for the water uptake reduction.
- The reinforcement was effective to enhance mechano-chemical stabilities.
- The composites showed higher durability than the bare ones in PEMFC, PEMWE.

GRAPHICAL ABSTRACT

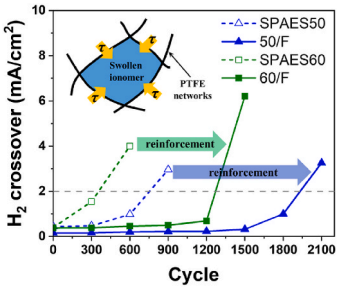

ARTICLE INFO

Keywords:
Reinforced membrane
Hydrocarbon-based ionomer
Fuel cell
PEMWE
Dilatation stress

ABSTRACT

The dimensional stability of proton exchange membranes in the moisture involved energy conversion devices polymer electrolyte membranes fuel cells (PEMFCs) and water electrolyzers (PEMWEs) is a critical property to prolong the cell life span. Here, highly water swellable sulfonated poly(arylene ether sulfone) (SPAES) ionomers are incorporated into mechanically tough porous poly(tetrafluoroethylene) (PTFE) to reduce the dimensional change in water. Three different SAPAES with a degree of sulfonation ranging from 40 to 60 are synthesized, and their composites with PTFE are prepared. The reinforced SPAES membranes show enhanced dimensional and mechanical properties due to the mechanical stress of the PTFE supports (~28 MPa) that oppose ionomer dilatation in water, which is evaluated from a thermodynamic perspective. The dimensionally stable composites show higher chemical stability in the *ex situ* Fenton's test and yield more stable long-term performance in both PEMFC and PEMWE, possibly due to reduced gas permeability and enhanced interfacial stability of the membrane electrode assembly. In the PEMFCs, the durability against wet–dry cycle at 80 °C is enhanced 3–4-fold, and in PEMWEs, the voltage increase over time at a constant current density of 2 A/cm^2 is significantly reduced by suppressing the ionomer's swelling in the confined PTFE frames.

* Corresponding author.
** Corresponding author.
E-mail addresses: dmyu@krict.re.kr (D.M. Yu), syso@krict.re.kr (S. So).
[1] These authors contributed equally.

https://doi.org/10.1016/j.jpowsour.2022.232221
Received 26 July 2022; Received in revised form 3 October 2022; Accepted 5 October 2022
Available online 17 October 2022

1. Introduction

Ion-conducting polymer electrolyte membranes (PEMs) are critical components of energy conversion and storage devices for maintaining cell performance without fuel loss in PEM fuel cells (PEMFCs), products in PEM water electrolyzers (PEMWEs), and active species in redox flow batteries [1–5]. In most energy conversion/storage devices that involve proton transfer processes, perfluorosulfonic acid (PFSA) ionomers, such as Nafion, are used for PEMs. This is because of their excellent proton conductivity, electrochemical stability, and mechanical toughness resulting from the distinctly phase-separated hydrophobic and hydrophilic domains and the mechanochemical properties of the poly(tetrafluoroethylene) (PTFE)-based polymer backbone [6–8]. Despite these advantages, high gas permeability and high production cost are major concerns that must be resolved for the wide commercialization of energy conversion/storage devices [9–11]. Various hydrocarbon-based ionomers have been developed to overcome the drawbacks of PFSA ionomers, particularly in terms of cost and gas permeability [12–15]. Because the densities of PFSA and hydrocarbon-based ionomers are different, the ion exchange capacity (IEC) of hydrocarbon-based ionomers must be approximately double that of PFSA ionomers to achieve a proton conductivity that is similar to that of PFSA ionomers.

A high IEC reduces the proton conduction resistance. However, it induces significant volume expansion in moisture involved PEMFCs and PEMWEs. Membrane swelling causes interfacial instability in membrane electrode assemblies (MEAs), and more importantly, accelerates the chemical and mechanical degradation of the membranes, even in the case of less swellable PFSA membranes. Hydrocarbon-based ionomers that have a higher IEC compared to PFSA ionomers show a larger degree of swelling and dimensional changes. In addition, they are more vulnerable to the damage caused by swelling-induced degradation, such as tears, cracks, pinholes, and chemical decomposition, which leads to cell failure [16–18]. While the imbibed water facilitates proton transport by interconnecting hydrophilic domains, it acts as highways for the crossover of fuels in PEMFCs or products in PEMWEs (H_2 and O_2) [19]. Gas crossover, which is undesirable, reduces the Faraday efficiency and induces the generation of reactive hydroxyl radicals [20]. In addition to percolation, the uptake of water expands the volume (area and thickness) of a PEM until the chemical potentials of ionomer-water mixing and ionomer deformation are balanced [21]. In systems that employ MEAs, this areal expansion causes interfacial instability between PEMs and catalyst layers (CLs) because of their swelling imbalance (PEM swells more than CLs). This leads to cracks in CLs and their delamination from PEMs or pinholes in PEMs, resulting in increased ohmic resistance [19,22].

Hydrocarbon-based ionomers have been incorporated into chemically inert and mechanically tough porous supports to reduce water uptake and dimensional changes (in length) [23–27]. This is one of the effective approaches for enhancing membrane durability [28–32]. Gore-Select membranes, Nafion XL, and HP are commercially available examples of PFSA-ionomer-based reinforced membranes with expanded porous PTFE [33–35]. PTFE fibers and knots prevent physical damage due to fatigue crack propagation and provide mechanical force to oppose the dilatation of constrained ionomers [36]. These features synergistically improve the chemical and physical durability of the membranes during cell operation, as compared to the corresponding bare PEMs [37,38].

Hydrocarbon-based ionomers have been reinforced with a porous layer to improve their durability in various applications. Miyake et al. prepared composite membranes with sulfonated polybenzophenone/poly(arylene ether) block copolymers and a porous polyethylene terephthalate layer. The composite showed significantly improved durability in a wet–dry cycling test for PEMFCs, with a 2.5 times lower water uptake at 80 °C [33]. Furthermore, they recently developed composite membranes with different combinations of an ionomer (sulfonated phenylated poly(phenylene) (SPP-QP)) and a porous support (porous polyethylene). The toughness of rigid SPP-QP was improved approximately ten-fold, and H_2 crossover was effectively reduced through reinforcement [39]. The enhanced properties facilitated the use of thinner membranes, which performed better than bare membranes. Kim et al. incorporated highly sulfonated poly(arylene ether sulfone) (SPAES), which showed a significant water uptake of over 400 wt% at 60 °C, into a poly(benzimidazole)-based substrate [40]. After pore filling, the composites were dimensionally stable even in hot water (30–35 wt% water uptake) and exhibited excellent mechanical properties and PEMFC performance. Most studies on reinforced membranes have mainly reported the effects of reinforcement on dimensional changes, mechanical properties, cell performance, and durability, typically for PEMFCs. However, the swelling behaviors and the relationship between swelling and the performance, properties after reinforcement have not been investigated in detail.

In this study, we synthesized three SPAESs with different IECs and used them as ionomers for three-layered composite membranes with porous PTFE. The degree of reinforcement was examined by comparing the water uptake, dimensional stability, and mechanical properties of the composite and bare membranes. The swelling behavior was investigated using Newman's membrane model under a constrained environment [41] to evaluate the stress provided by the PTFE networks, which prevented membrane swelling in water. The reinforcement was effective in decreasing membrane swelling and H_2 permeation and increasing mechanical toughness and chemical stability. These enhancements synergistically yielded stable long-term performance in PEMFCs and PEMWE cells.

2. Experimental

2.1. Materials

A porous PTFE substrate (porosity >80% and thickness of 9–10 μm) was purchased from SYNOPEX. 4,4′-Dihydroxybiphenyl (BP) and 4,4′-difluorodiphenyl sulfone (DFDPS) were purchased from Songwon and Richem, respectively. BP and DFDPS were recrystallized from ethanol prior to use. DFDPS was utilized to synthesize 3,3′-disulfonated-4,4′-difluorodiphenyl sulfone (SDFDPS) using fuming sulfuric acid (65%, Merck Specialties Private Limited) based on a previously reported procedure [42]. The resulting SDFDPS was purified by recrystallization from water and ethanol. Potassium carbonate (K_2CO_3) was purchased from Sigma-Aldrich and dried under vacuum at 80 °C for 24 h prior to use. *N*-methyl-1-pyrrolidone (NMP) and toluene were purchased from Sigma-Aldrich and used as received. 1-Propanol (NPA) was purchased from Samchun Chemicals and used as received. IrO_2 powder was purchased from Boyaz Energy, and a Pt/C catalyst (46.6 wt% Pt) was purchased from Tanaka Kikinzoku Kogyo. Nafion dispersions (D2021 and D521) and membranes (Nafion 211, 212, and HP) were purchased from Chemours. Nafion 212 and 211 were cast membranes with thicknesses of 50.0 ± 0.8 μm and 25.5 ± 0.2 μm, respectively, and Nafion HP (NHP) was a reinforced membrane with a thickness of 29.1 ± 0.3 μm. All the Nafion membranes were used as received without pretreatment.

2.2. Synthesis of SPAES

As shown in Fig. 1a, SPAES was synthesized through the condensation polymerization of BP, DFDPS, and SDFDPS. A Dean–Stark trap, condenser, mechanical stirrer, and nitrogen inlet were installed in a 4-neck round bottom flask, and then, BP, DFDPS, and K_2CO_3 were added to an NMP/toluene mixture (v/v ratio 1:1). The mixture was slowly heated to 160 °C for 2 h and then refluxed for 4 h to azeotropically dehydrate the reaction system. Next, the temperature was increased to 185 °C for 2 h to remove toluene. Subsequently, SDFDPS and supplementary NMP were added to the reactor, the reaction temperature was raised to 195 °C, and the reaction progressed for an additional 13 h. The reactor was cooled, and the obtained product was

washed twice with deionized water and isopropyl alcohol to eliminate NMP, unreacted monomers, and byproducts. Finally, synthesized SPAES was dried in a vacuum oven at 80 °C for 48 h. The input molar ratios of DFDPS and SDFDPS were controlled to obtain SPAES with degrees of sulfonation (DSs) of 40%, 50%, and 60%, which were denoted as SPAES40, SPAES50, and SPAES60, respectively.

The molecular weights of the SPAESs were measured using gel permeation chromatography (GPC, YOUNG IN Cromass) with a UV/visible detector. GPC samples (2 mg/mL) were prepared in *N*,*N*-dimethylacetamide with 0.05 M LiBr. The prepared samples were injected into the GPC column at 50 °C at a rate of 1 mL/min using a pump. The obtained chromatogram was calibrated using polystyrene references to determine the molecular weight. The inherent viscosity (η_{inh}) was measured using a Cannon Ubbelohde viscometer with a polymer solution in NMP at a concentration (c) of 2 mg/dL. The times required by pure NMP (t_s) and the polymer solution (t_p) to pass through the capillary tube were measured, and η_{inh} was obtained from the following equation:

$$\eta_{inh} = (\ln\eta_r)/c = \ln(t_p/t_s) \times (1/c). \quad (1)$$

2.3. Preparation of pristine and pore-filled SPAES membranes

SPAES was dissolved in NMP (15 wt%) and the solution was cast on a glass plate and transferred to a convection oven at 80 °C for 6 h to prepare pristine SPAES membranes. As illustrated in Fig. 1c, pore-filled membranes were prepared by placing a porous PTFE (10 cm × 10 cm) support onto the cast area, followed by NPA spraying for PTFE treatment. The glass plate was placed on a hot plate at 70 °C for 1 h. Thereafter, another SPAES solution layer was cast onto the composite to obtain a symmetric composite membrane along the thickness direction. Similar to the pristine membranes, the composite membranes were dried in a convection oven at 80 °C for 6 h. All membranes were protonated by soaking them in 1.5 M H_2SO_4 for 24 h and washed with deionized water to remove residual acid. The protonated membranes were dried under vacuum at 80 °C for 24 h prior to use. The pristine membranes were named after the synthesized SPAES; the composite membranes containing SPAES with a DS of 40%, 50%, and 60% were named 40/F, 50/F, and 60/F, respectively. The target thickness for all the membranes was 30 μm.

2.4. Membrane characterization

2.4.1. IEC

The IEC of a membrane was measured using the titration method. The weight of the completely dried membrane was measured, and the membrane was immersed in a 0.01 M NaCl solution (100 mL) for 24 h under continuous stirring. The released protons were titrated with a 0.01 M NaOH solution with a pH meter, and the IEC value was calculated using Equation (2).

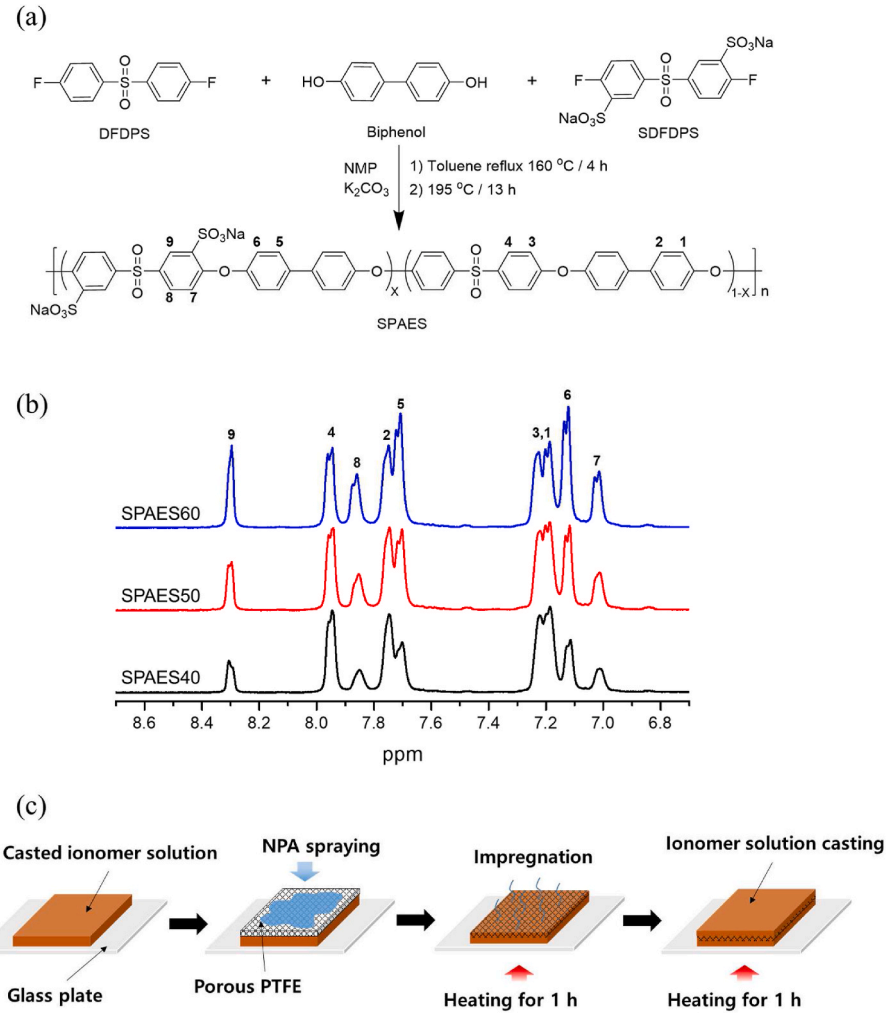

Fig. 1. (a) General synthesis scheme for SPAES ionomers. (b) ^{1}H NMR spectra of SPAES ionomers in DMSO-d_6. (c) Schematic illustration of the reinforced SPAES membrane preparation.

$$IEC = (V_{NaOH} \times C_{NaOH})/w_m, \quad (2)$$

where V_{NaOH} is the input volume of NaOH, C_{NaOH} is the NaOH concentration (0.01 M), and w_m is the weight of the dried membrane.

2.4.2. Dimensional changes

Changes in the weight and dimensions of the membranes upon swelling in water were quantified in terms of the changes in the water uptake (ΔW), length (ΔL), and thickness (ΔT). These were obtained by comparing the values obtained after swelling to those obtained after the membranes were completely dried under vacuum at 80 °C for 24 h. The dried membranes were immersed in a water bath for at least 5 h at the desired temperature to achieve equilibrated swelling.

2.4.3. Mechanical properties

Mechanical properties were evaluated using a universal testing machine (LR5k, Lloyd Instruments). Fully dried and swollen samples were prepared and cut according to the ASTM standard D638V. The measurement was conducted at a crosshead speed of 5 mm/min under ambient conditions.

2.4.4. Chemical stability

The *ex situ* Fenton test was carried out to determine the chemical stability of the membranes to hydroxyl radicals. The dried membranes with similar thicknesses (~30 μm) were cut into samples with dimensions of 1 cm × 3 cm and immersed in Fenton's solution containing 3% H_2O_2 and 2 ppm Fe^{2+} ($FeSO_4$) at 60 °C for 6 h without any mechanical disturbance. The reacted membranes were filtered and washed with deionized water and vacuum dried at 80 °C for 24 h. The weight of the remaining membranes was measured to calculate the weight loss (%) of the membranes with respect to the initial weight.

2.4.5. Proton conductivity

The proton conductivity in liquid water was evaluated using impedance spectroscopy (Solartron 1280 AC) with a four-point probe cell. All the samples (1 cm × 3 cm) were equilibrated in deionized water for at least 2 h before the measurements. The proton conductivity was evaluated using the same cell configuration and various humidity conditions (20%–100% RH at 80 °C) using impedance spectroscopy (PGZ 301 dynamic electrochemical impedance spectroscopy voltammeter, BekkTech).

2.4.6. H_2 permeability

The H_2 permeability (P) was evaluated by measuring the permeated H_2 across a membrane in carrier gas (Ar) flow using a gas chromatography (YL6500 GC, Young In) equipped with a thermal conductivity detector (Equation (3)). The membrane was exposed to humidified H_2 and Ar flows at 80 °C and 100% RH. The cell temperature and the temperature and humidity of the gases were controlled by a fuel cell station (SFC-TS, Fuel Cell Technologies Inc.), which was connected to the chromatograph.

$$P = (C_H \times v \times t) / (A \times \Delta p), \quad (3)$$

where C_H is the measured concentration of H_2 in Ar, v is the Ar flow rate, t is the membrane thickness, A is the area exposed to humid gases, and Δp is the H_2 partial pressure difference across the membrane.

2.5. MEA preparation and single-cell performance

2.5.1. CL preparation for MEA

The catalyst slurry for the anode in the MEA of a PEMWE was prepared using IrO_2 powder, a Nafion dispersion solution (D2021), and NPA. The weight ratio of IrO_2 to the Nafion ionomer was 9:1, and the solid content was 40%. A Pt/C catalyst and Nafion dispersion solution (D521) were used to prepare the catalyst slurry for the cathode in the MEA of the PEMWE and the electrodes in the MEA of a PEMFC. The weight ratio of Pt/C to the Nafion ionomer was 3:1, and the solid content was 17%. The catalyst dispersions were mechanically mixed at 400 rpm for 2 h, and then sonicated for 10 min using an ultrasonicator (VCX 750, Sonics & Materials), which was alternately switched on and off for 5 s. A doctor blade was used to cast the dispersions onto a fluorinated polyimide film at a speed of 15 mm/s. Next, the CL was dried in a convection oven at 70 °C and stored in a desiccator before use.

2.5.2. MEA preparation

The prepared electrodes were transferred to a membrane using the decal transfer method. A sandwiched assembly with the anode, cathode layers, and membrane was hot pressed at 130 °C under a pressure of 58.8 MPa for 10 min. The active area was 5 cm^2, and the loadings of IrO_2 and Pt/C were 2.0 ± 0.3 mg/cm^2 and 0.35 ± 0.05 mg/cm^2, respectively.

2.5.3. Single-cell performance

The PEMFC single cell was operated at 80 °C under 25%, 50%, and 100% RH and ambient pressure. H_2 and air were supplied to the anode and cathode, respectively, at a stoichiometric ratio of 1.5:2. The MEAs were activated by cycling the voltage was between 0.3, 0.6, and 0.9 V, where each voltage was maintained for 3 min. The cycle was performed 24 times. After the MEA conditioning, the current density was recorded from 1.0 to 0.3 V at a voltage scanning rate of 0.05 V/25 s to obtain polarization curves. The PEMWE single cell was operated at 80 °C under ambient pressure with the continuous water flow at 30 mL/min to the anodic side. The MEAs of the PEMWE cell were conditioned by maintaining the cell voltage at 1.55 V for 30 min. The polarization curves of the PEMWE cell were obtained by recording the current density corresponding to applied voltages of 1.35–2.0 V at a scanning rate of 0.05 V/30 s. It should be noted that carbon papers (Sigracet 39BCE, 325 ± 25 μm thick) were used as gas diffusion layers for both electrode sides in the PEMFC single cells and for the cathode side in the PEMWE single cells. A platinum-coated porous transport layer (LT Metal, 400 ± 20 μm thick) was used on the corrosive anode side with a high electrochemical potential in the PEMWE single cells.

2.5.4. Durability test

The wet–dry durability test was performed for the membrane mechanical cycle in the PEMFC according to the US DOE protocol [43]. The gas flow rates (H_2 for the anode and N_2 for the cathode) were maintained at 1000 sccm, and the humidity was alternately varied between 150% RH for 2 min and 0% RH for 2 min at 80 °C until the H_2 crossover current density exceeded 2 mA/cm^2. The H_2 crossover current density was measured at 80 °C and 100% RH using linear sweep voltammetry (LSV). Every 300 wet–dry cycles, the cell voltage was increased from 0 to 0.6 V at a rate of 2 mV/s using a potentiostat (BioLogic). For the PEMWE, the membrane durability during cell operation was tested at a constant current density of 2 A/cm^2 for 100 h, and the corresponding voltage change was monitored to determine the degradation rate.

3. Results and discussion

3.1. Synthesis of IEC controlled SPAES series

SPAES ionomers were prepared through the condensation polymerization of BP, DFDPS, and SDFDPS, as shown in Fig. 1a. The DS was controlled from 38.0% to 58.5% by varying the ratio of DFDPS and SDFDPS (Table 1), and it was calculated using the ^1H NMR integration values of H_9 and H_4. The ^1H NMR spectra of dimethyl sulfoxide (DMSO-d_6) (Fig. 1b) showed that the peaks of H_9, H_8, and H_7 were noticeably enhanced compared to the normalized peak of H_4 with increasing DS. The IECs of SPAES40, SPAES50, and SPAES60 were 1.59, 1.93, and 2.25 meq/g, respectively (see Table 2). All SPAESs were successfully synthesized with a high molecular weight (M_n) of over 150 kg/mol (higher than 10 times the entanglement molecular weight of SPAES

(~10 kg/mol)). The characteristics of the SPAES series are listed in Table 1.

3.2. IEC analysis of the composite membranes

We recently developed a facile method for tuning the surface energy of PTFE substrates by spraying them with NPA [44]. The contact angle of the SPAES50 solution (15 wt% in NMP) on the PTFE substrate decreased from 129° to 67.2° after the NPA treatment. As a result, a more translucent SPAES50/PTFE composite membrane was prepared with less void formation during the SPAES solution infiltration process. This method was used to incorporate the SPAES40, SPAES50, and SPAES60 ionomers into porous PTFE substrates, and three-layered composite membranes were prepared (40/F, 50/F, and 60/F). The cross-sectional SEM images of 50/F are shown in Fig. S1. Similar to the pristine membranes, the total thickness of the composite membranes was approximately 30 μm (see Table 2). The reinforced layer was located in the middle of the composite membranes, and the top and bottom layers were composed of bare SPAES ionomers, similar to the composites with PFSA ionomers.

The IEC of the composite membranes was expected to be lower than that of the bare membranes because of the nonfunctional PTFE support. The theoretical IEC (IEC_{theo}) of a composite membrane was evaluated using the following equation:

$$IEC_{theo} = IEC \times (\rho_i V_i + \rho_i \Phi V_r) / w_{com}, \quad (4)$$

where V_i and V_r are the volumes of the SPAES and reinforced layers, respectively, Φ is the porosity of the PTFE substrate, and w_{com} is the total weight of the composite membrane. Assuming perfect infiltration without vacancies in the composite membrane, IEC_{theo} was expressed as

$$IEC_{theo} = IEC \times (2 \rho_i l_i A + \rho_i l_r A \Phi) / (2 \rho_i l_i A + \rho_r l_r A), \quad (5)$$

where l_i and l_r are the thicknesses of the SPAES and reinforced layers, respectively (see Fig. S1), and ρ_r is the density of the reinforced layer calculated using the densities of SPAES (ρ_i) and PTFE (ρ_{PTFE}) ($\rho_r = \Phi \rho_i + (1 - \Phi) \rho_{PTFE}$) (see Table S1). The thicknesses of PTFE and the composites were $l_i = 10$ μm and $l_{tot} = 2 l_i + l_r = 30$ μm, respectively. Thus, the estimated values of IEC_{theo} were 1.40, 1.71, and 2.00 meq/g for 40/F, 50/F, and 60/F, respectively, which were remarkably close to the experimental results (Table 2). This showed that the SPAES solutions infiltrated the PTFE pores without significant void formation through the solvent treatment, even though the SPAES ionomers and PTFE were not chemically compatible with each other.

3.3. Dimensional stability and constraining stress

The reinforcement in this study does not exhibit in-plane anisotropy in membrane swelling (Fig. S2) due to the isotropic characteristics of the substrate in terms of pore geometry and mechanical properties. As evident from the surface SEM images (Fig. S3), the pores are uniformly distributed and do not show clear differences in their geometries depending on the direction, machine direction (MD) and transverse direction (TD). Based on an advanced capillary flow porometer analysis with a Galwick solution, the mean pore diameter was 0.23 μm with a standard deviation of 0.01 μm (Fig. S4b). In the tensile experiments, the mechanical properties (modulus, tensile strength, and elongation at break) of the substrate are similar in both MD and TD (Fig. S4a). Because of this isotropy in the mechanical properties of the substrate, and in the swelling behavior of the reinforced membranes, all measurements were conducted without considering the in-plane direction of the substrate.

Table 1
Characteristics of SPAES ionomers.

	DS (%)	M_n (kg/mol)	M_w (kg/mol)	$Đ$	η_{inh} (dL/g)
SPAES40	38.0	169.8	326.0	1.92	2.60
SPAES50	48.6	180.8	352.8	1.95	2.67
SPAES60	58.5	160.9	304.1	1.89	2.44

Table 2
Characteristics of membranes.

Membrane	Thickness (μm)	IEC [a] (meq/g)	ΔW [b] (wt. %)	ΔL [c] (%)	Toughness (MJ/m^3) [d]	
					dry	wet
SPAES40	30.3 ± 0.6	1.6 ± 0.0077	56.2 ± 0.7	16.7 ± 1.2	57 ± 16	39 ± 13
SPAES50	32.2 ± 1.0	1.9 ± 0.0061	111.1 ± 0.7	35.3 ± 0.5	59 ± 14	35 ± 11
SPAES60	32.4 ± 0.9	2.3 ± 0.0033	277.6 ± 20.0	74.6 ± 2.1	59 ± 10	33 ± 5
40/F	30.8 ± 1.1	1.4 ± 0.0030	31.2 ± 3.6	12.7 ± 0.1	73 ± 22	48 ± 5
50/F	32.6 ± 1.2	1.7 ± 0.0074	52.6 ± 2.0	21.4 ± 0.9	71 ± 20	43 ± 3
60/F	30.9 ± 1.2	2.0 ± 0.0058	137.0 ± 13.6	31.1 ± 0.6	70 ± 18	36 ± 2
Nafion211	26.0 ± 0.5	0.9 ± 0.0044	28.1 ± 0.6	14.8 ± 0.7	37 ± 7	19 ± 3

[a] Ion exchange capacity of the membranes obtained via the titration method.
[b] Water uptake at 80 °C.
[c] Dimensional change in length at 80 °C.
[d] Toughness was evaluated by integrating the stress–strain curves of the dried and fully swollen membranes at room temperature.

At 25–80 °C, the water uptake of SPAES increased with the DS because the number of hygroscopic sulfuric acid groups increased. It has been previously reported that the water uptake abruptly increases above a certain DS (50% in this study), where the hydrophilic domains start to be percolated [19,45]. For example, at 80 °C, the SPAES60 membrane absorbed approximately 280 wt% water, which was 2.5 times higher than the water absorbed by SPAES50. After reinforcement, the water uptake of the composite membrane with the SPAES ionomer increased with the DS, as shown in Fig. 2a. The water uptake of the composite membranes was approximately half of that of the bare membranes. This was expected because the water uptake decreased with the IEC. However, when the water uptake was plotted as a function of the IEC, the water uptake of the reinforced membranes was lower than the value of connecting lines from the water uptake of the bare membranes at a certain IEC (Fig. S5). This showed that there is an additional reduction effect over a lowering of the IEC in the water uptake resulting from the reinforcement.

Hydrophilic sulfonic acid groups generally cause a PEM to attract water molecules. However, according to the simple Flory–Rehner theory for the swelling behavior of a polymer network, the amount of water molecules absorbed by a sulfonic acid group is mainly limited by elastic friction driven by the elasticity of the ionomer at equilibrium [21,46]. Considering that the pore-filled ionomers are constrained by well-connected PTFE networks, as shown in Fig. 3a, the additional reduction in the water uptake can originate from the mechanical stress (τ) caused by PTFE networks, which acts opposite to the outward direction of ionomer swelling. Thermodynamically, Meyers and Newman reported the swelling behavior of a PEM through the equilibrium state of water within the PEM in a typical fuel cell based on the multicomponent Gibbs function [47,48]. Furthermore, by incorporating an external stress term, they developed a mathematic model to estimate the water content and its activity in the constrained PEM under typical PEMFC operating conditions [41]. At equilibrium, the chemical potentials ($\mu^{(2)}$ and $\mu^{(3)}$) of water in the freely swollen membrane (state 2 in Fig. S6) and swollen reinforced membrane (state 3 in Fig. S6) were considered to be the same according to Newman's approach (Equation (6)) if the stress applied by the PTFE networks (τ, Fig. 3a) was considered instead of the dilatation stress (τ_d) generated by compression during cell assembly. Then, because $\mu^{(2)}$ was equal to $\mu^{(3)}$, the chemical potential change ($\Delta\mu_0$) was expressed as

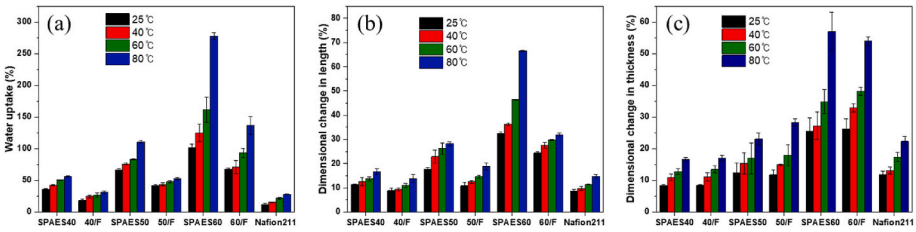

Fig. 2. (a) Water uptake and dimensional changes in (b) length and (c) thickness directions of the SPAES and reinforced membranes in liquid water at various temperatures from 25 to 80 °C.

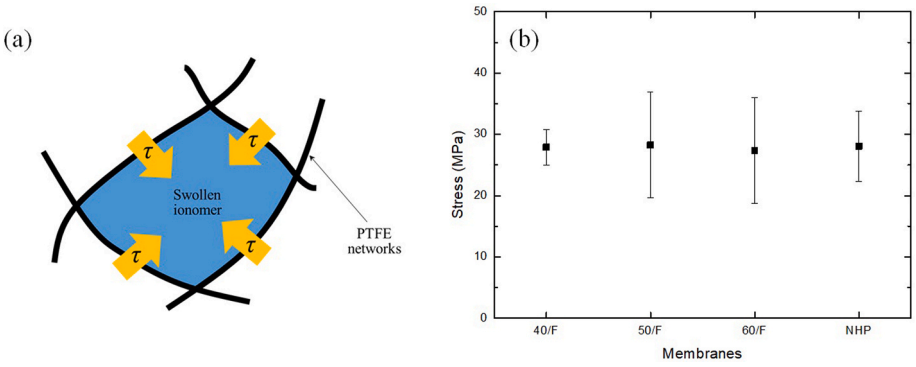

Fig. 3. (a) Schematic illustration of the ionomers constrained by PTFE networks, and (b) stress (τ) as a function of the ionomer swelling in liquid water.

$$\Delta\mu_0 = RT\,\Delta\ln\lambda + V_0\,\tau = 0, \tag{6}$$

where R is the gas constant, T is the absolute temperature, λ is the number of water molecules per sulfonic acid group, and V_0 is the molar volume of water at temperature T. As the values of λ for the freely swollen membrane (λ_f) and swollen reinforced membrane (λ_r) were experimentally measurable on the basis of the IEC and water uptake, the mechanical stress of the PTFE supports (τ) was expressed as

$$\tau = -\frac{RT}{V_0}\ln\left(\frac{\lambda_r}{\lambda_f}\right). \tag{7}$$

The values of λ were experimentally obtained using the IEC and water uptake, as summarized in Table S2, and the stress values preventing the swelling of the ionomer was evaluated at various temperatures using Equation (7). It should be noted that the modulus of semicrystalline PTFE did not vary significantly within the temperature range of 25–80 °C according to thermomechanical analysis [49]; hence, the values of τ at different temperatures were averaged for a reinforced membrane. As shown in Fig. 3b, the stress exerted on the swollen SPAES ionomers by the PTFE networks was approximately $\tau = 28$ MPa, which was equivalent to the external pressure required to shrink a freely swollen membrane. The value of τ was similar to that of a composite membrane (NHP) composed of Nafion ionomers and porous PTFE ($\tau = 28.0 \pm 5.7$ MPa). This suggested that the constraining stress could be more closely related to the type of porous supports than to the ionomers.

To determine the reduction in the water uptake of the composite membranes in different directions, the dimensional stabilities in the length (ΔL) and thickness (ΔT) directions were investigated in addition to the weight-based swelling behavior. As shown in Fig. 2b and c, after the reinforcement, the dimensional changes in the length were significantly reduced while the changes in the thickness were not. This was due to the anisotropic pore morphology of the expanded PTFE substrate caused by the manufacturing process and the biaxial mechanical expansion of the PTFE membrane (Fig. S3). During the expansion process, PTFE fibrils were more aligned along the in-plane directions, and thus, open pores were predominantly formed along the thickness direction. Therefore, the constrained ionomers could swell to a greater extent along the through-plane direction without significant opposing stress by the PTFE fibrils. For example, the values of $\Delta T/\Delta L$ for SPAES60 and 60/F at 80 °C were 0.86 and 1.69, respectively. A similar trend was reported in previous studies on Nafion/PTFE composite membranes [50, 51].

3.4. Mechanical properties

A recent study on Nafion XL reported that nonfunctionalized PTFE supports were mechanically stronger than PFSA ionomers with the same polymer PTFE backbone [50]. Shi et al. estimated the Young's modulus of PTFE as 0.8–2 GPa using the rule of mixtures and that of Nafion 211 as only approximately 250 MPa. The high Young's modulus of the PTFE fibrils was also effective in reinforcing the engineering-plastic-based SPAES membranes, as shown in Fig. 4a and b. The Young's modulus of the bare SPAES membranes was 470–650 MPa in the dried state and that of the composite membranes was 580–740 MPa (the Young's modulus increased with the DS). A similar trend was observed in the tensile strength behavior after reinforcement (Fig. 4b). The Young's modulus of the PTFE fibrils estimated according to the rule of mixtures was approximately 2 GPa, which was similar to the modulus of PTFE along the MD [50]. The elongation at break in the dried state did not increase after the reinforcement (Fig. 4c) because the elongation at break of PTFE (113.0 ± 37.5%) was lower than that of the bare SPAES membranes (~200%). During the PEMFC and PEMWE cell operations, PEMs are continuously exposed to wet conditions. Thus, PEMs must be mechanically tough in both swollen and dry states. Fig. 4 shows the comparison of the mechanical properties of the swollen and dry membranes. The general trend of the variation in the Young's modulus and tensile strength for the swollen membranes was similar to that for the dry membranes. However, the absolute values for the swollen membranes were lower because a large amount of water was incorporated into the membranes, which was acceptable according to the rule of mixtures [52]. The elongation at break for the reinforced membranes did not vary significantly after swelling. However, it decreased by more than 100% for the membranes with high IEC values (SPAES50 and SPAES60) (Fig. 4c). As a result, the mechanical toughness of the

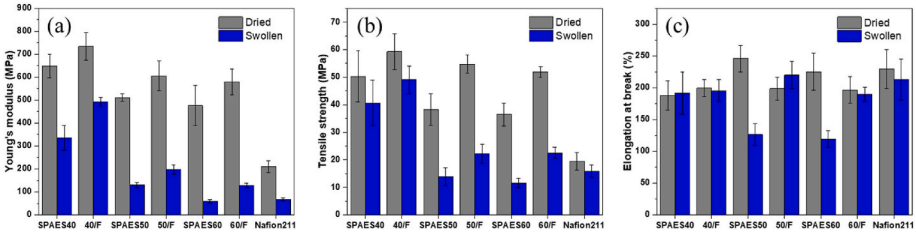

Fig. 4. (a) Young's modulus, (b) tensile strength, and (c) elongation at break of the dried and swollen membranes at room temperature.

reinforced membranes (~58 MJ/m^3 in the dried state and 36–48 MJ/m^3 in the swollen state) was higher than that of the bare membranes (~70 MJ/m^3 in the dried state and 33–39 MJ/m^3 in the swollen state), as shown in Table 2.

3.5. Ex situ chemical stability

In PEMFC and PEMWE applications, hydroxyl radicals (HO•) are the main causes of the decomposition of PEMs because they attack the main chain close to the sulfonic acid groups and ether linkages in SPAES ionomers [53,54]. Fenton's test was conducted to evaluate the oxidative stability of SPAES and its composite membranes. As shown in Figs. S7 and S8, the composite membranes maintained their shape, whereas the pristine SPAES membranes disintegrated after Fenton's test (at 60 °C for 6 h). As the DS increased, the weight loss of the bare membranes increased from 15.8% (SPAES40) to 79.4% (SPAES60) after Fenton's test (Fig. 5). The weight loss of the membranes after reinforcement was significantly lower than that of the corresponding bare membranes. On the basis of the weight fraction (~11%) and the negligible weight loss (1.6%) of PTFE after Fenton's test, the weight loss of the reinforced membranes was estimated under the assumption that the degradation rate of the SPAES ionomers did not change after reinforcement. The estimated values (13.9%, 26.5%, and 70.6% weight loss for 40/F, 50/F, and 60/F, respectively, shown in Fig. 5) were approximately 1.5 times higher than the experimental results. This indicated that the reinforced membranes were chemically more stable than the bare membranes to a greater extent than the theoretical estimation solely due to the chemically inert PTFE. This synergistic enhancement in the chemical stability was explained from the viewpoint of chemical reactions. First, the chemically inert PTFE substrate probably prevented the reactions between hydroxyl radicals and ionomers by providing physical transportation barriers for the reactive radicals in the reinforced membranes soaked in Fenton's solution. Second, the concentration of reactive species in the reinforced membranes might have been reduced owing to the decreased water uptake. The concentrations of H_2O_2 and Fe^{2+} in the membranes were calculated by assuming that the water uptake was similar to the uptake obtained from Fenton's solution. Because H_2O_2 and Fe^{2+} are the main reactants for hydroxyl radical formation ($H_2O_2 + Fe^{2+} \rightarrow Fe^{3+} + HO\bullet + HO^-$), the concentration of the species is proportional to the ionomer degradation reaction rate (HO• + (ionomer) → (decomposed products)) [55]. The estimated H_2O_2 and Fe^{2+} concentrations in the less swellable reinforced membranes were approximately 1.5 times lower than those in the corresponding bare membranes. Moreover, there was a linear correspondence between the water uptake and the weight loss after Fenton's test, as shown in Fig. S9.

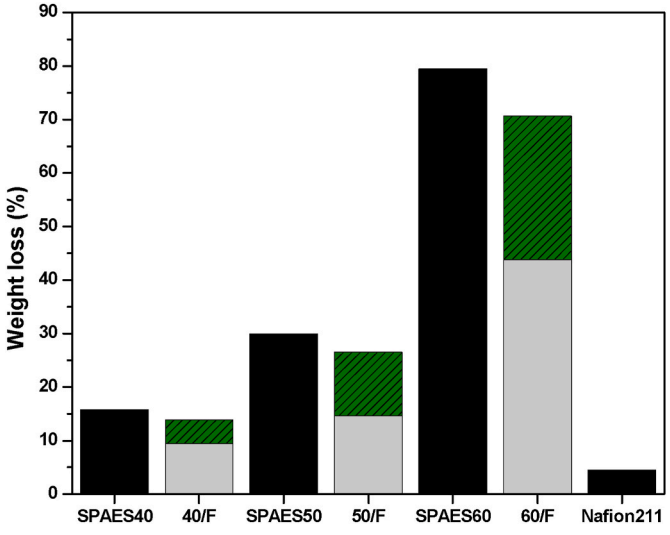

Fig. 5. Weight loss of the membranes after Fenton's test at 60 °C for 6 h. Shaded green regions of the reinforced membranes represent the difference between the theoretically estimated and experimental degradation values of weight loss. (For interpretation of the references to colour in this figure legend, the reader is referred to the Web version of this article.)

However, the chemical stability of the SPAES-based membranes is poorer than that of Nafion 211 according to the weight loss in Fenton's solution (Fig. 5), even after reinforcement. To enhance the chemical stability of hydrocarbon-based membranes, the chemical structure of ionomers should be designed without chemical weak points in the polymer chains. For example, the design of polyphenylene-based PEMs with no ether linkages, which result in chemical degradation owing to the formation of hydroxyl radicals, have been described [56–59]. These studies demonstrate that ether-free ionomers show high proton conductivity, reasonable mechanical and chemical stability, and low gas permeability. In addition, polyphenylene-based PEMs exhibit reasonably high fuel-cell performance under practical conditions.

3.6. Proton conductivity and cell performance

Proton conductivity is a critical material property that determines the performances of PEMFC and PEMWE cells. A higher proton conductivity is desirable for obtaining a higher current density at a specific voltage by reducing the ohmic potential drop. The proton conductivity for PEMFC and PEMWE applications was measured at 80 °C under various humidity conditions. As shown in Fig. 6a, the in-plane proton conductivity (σ_i) of the reinforced membranes was lower than that of the bare membranes because of their lower IEC values and the nonionic PTFE barrier. However, in liquid water, the difference between the proton conductivities of the reinforced and bare membranes was not significant. The through-plane proton transport behavior, which directly represented the cell performance, was examined by measuring the high-frequency resistance (HFR) of the PEMFC and PEMWE single cells of all the membranes under various conditions (Fig. S10). The HFR is closely related to the through-plane proton conductivity ($\sigma_t \sim t/(\text{HFR})$, where t is the membrane thickness). The non-PEM resistance should be subtracted from the HFR to accurately evaluate σ_t. Nonetheless, the values of $t/(\text{HFR})$ are useful for determining the proton conductivity of the membranes under the assumption that the non-PEM resistance does not vary significantly. As shown in Fig. 6b, similar to the in-plane proton conductivity, the reinforced membranes showed satisfactory through-plane proton conductivity compared to the bare membranes at 100% RH and in liquid water at 80 °C. However, the values decreased with the

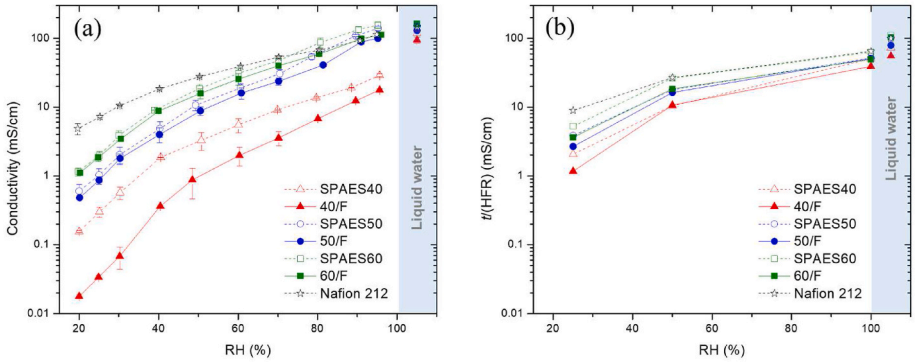

Fig. 6. (a) Proton conductivity and (b) the ratio of membrane thickness and high frequency resistance (t/(HFR)) of the SPAES and composite membranes under various humidity conditions at 80 °C.

humidity, which might be due to a sufficient number of proton carriers (water molecules) at higher relative humidity. For example, the ratios of t/(HFR) values for SPAES60 to 60/F at 25% RH and under liquid water flow were 1.44 and 1.08, respectively.

To exclude the effect of the thickness on the cell resistance, membranes with similar thicknesses (~30 μm) were used to evaluate the PEMFC and PEMWE performance. The catalyst loading was almost identical for all membranes (the loading of IrO_2 was 2.0 ± 0.3 mg/cm^2 and that of Pt/C was 0.35 ± 0.05 mg/cm^2). The outer surface of the membranes that was in contact with the electrodes was composed of the pristine ionomers. Thus, the difference between the performances of the cells with an SPAES membrane and its corresponding reinforced membrane was mainly caused by the interfacial instability in the MEAs during operation and the proton conductivity of the membranes. The polarization curves of PEMFC single cells at 80 °C and 25%, 50%, and 100% RH are shown in Fig. 7a–c. The performance of the single cells with the bare membranes was better than that of the cells with the reinforced membranes for all humidity conditions. However, at 100% RH, there was no considerable decrease in the performance for the single cell comprising reinforced membranes because of the proton transport behavior. At 25% RH, the current density of the PEMFCs with the bare membranes (0.10–0.34 A/cm^2) was higher than that of the PEMFCs with the composite membranes (0.09–0.20 A/cm^2) at 0.4 V. However, at 100% RH, the current density of the cells with the bare membranes (1.57–1.85 A/cm^2) was similar to that of the cells with the composite membranes (1.56–1.77 A/cm^2) at 0.4 V. When the membranes were exposed to the liquid water flow in the PEMWE single cells, the performance of the reinforced membranes was similar to or slightly better than that of the bare membranes, as shown in Fig. 7d. The current density of the cell with SPAES60 was 9.1 A/cm^2 at 2.0 V while that of the cell with 60/F having lower IEC value than SPAES60 was 9.6 A/cm^2. This result might be due to similar proton conductivities in liquid water and the membrane-thickness-sensitive cell performance. As shown in Fig. 6, the proton conductivity in liquid water was not significantly reduced by incorporating PTFE supports. Thus, the membrane thickness should be carefully considered to determine the effect of the reinforcement on the cell performance. For example, the membrane thicknesses of 60/F and SPAES60 were 32.7 and 34.8 μm, respectively (see Table S3

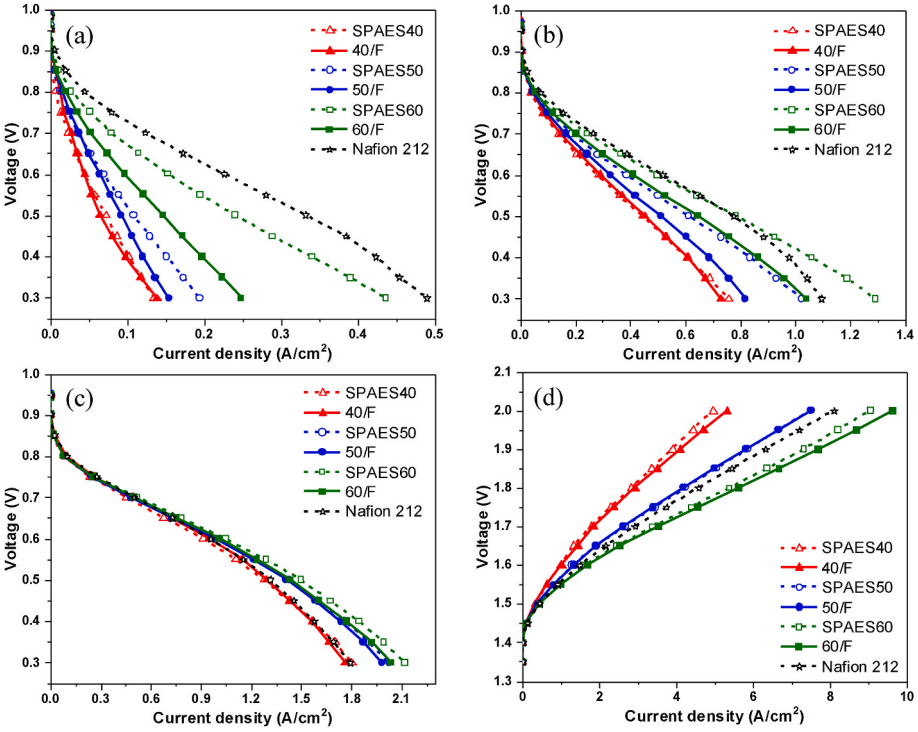

Fig. 7. PEMFC single cell performance at (a) 25%, (b) 50%, and (c) 100% RH and (d) PEMWE single cell performance of the pristine SPAES and reinforced membranes. The single cells were operated at 80 °C.

for the membrane thicknesses). The values of the in-plane proton conductivity and membrane thickness were used to determine the areal resistance, which is a key factor in determining the cell performance. The areal resistance of 60/F and SPAES60 was ca. 20.2 and 21.3 mΩ cm^2 at 80 °C, respectively. The PEMFC and PEMWE cell performance results showed that reinforcement did not affect the cell performance under high-humidity conditions for the PEMFCs and the wet condition for the PEMWEs, even though the sulfonic acid content of the reinforced membranes was lower than that of the original ionomer-based membranes.

3.7. PEMFC and PEMWE durability

The effect of the reduction in swelling on the membrane durability was examined by utilizing the pairs of SPAES50 / 50/F and SPAES60 / 60/F membranes, which showed distinctly enhanced dimensional stability as a result of the reinforcement, in the PEMFC and PEMWE. Durability tests, wet–dry cycling in the PEMFC, and constant current density operation in the PEMWE were used to determine the membrane durability, particularly *in situ* mechanical and chemical degradation. It has been reported that confined and fixed membranes with electrodes and cell assemblies experience extreme mechanical stress under humidity cycles (150% and 0% RH at 80 °C), which leads to mechanical failures [33,60]. Mechanical failures, such as pinholes, cracks, and other physical defects in PEMs, can be detected through gas leakage tests. Humidified H_2 was flown to the anode side of a PEMFC single cell every 300 wet–dry cycles, and the H_2 leakage to the other side was monitored using LSV at 80 °C and 100% RH. The physically durable number of cycles (N) was determined based on the target, where the H_2 crossover current density (i_x) exceeded 2 mA/cm^2, as proposed by the US DOE [43]. As summarized in Fig. 8a, the physical durability under harsh wet–dry conditions was significantly improved through the reinforcement. Although the values of N were conservatively read, 50/F ($N \approx$ 1800) and 60/F ($N \approx 1200$) were more durable than SPAES50 ($N \approx 600$) and SPAES60 ($N \approx 300$). This was attributed to the improved dimensional stability and mechanical toughness of the membranes due to the reinforcement. The mechanical stress of the PTFE supports (~28 MPa) in the direction opposite to ionomer dilatation in water might have contributed to the reduction in the effective internal stress, particularly for swollen membranes.

In PEMWE cells, H_2 and O_2 crossover should be minimized to prevent the explosion of gas mixtures, to enhance the Faraday efficiency, and to prevent the chemical degradation of PEMs [61]. The gas permeability of SPAES ionomers is less than that of PFSA ionomers, even in a highly swollen state [19,62,63]. For example, at 80 °C and 100% RH, the H_2 permeability (P) of Nafion 211 was 117.1 barrer while that of highly swellable SPAES60 was 63.6 barrer (Fig. S11). The good gas barrier property of the SPAES ionomers was further improved through the reinforcement, as shown in Fig. S11. The H_2 permeability values of Teflon and dried Nafion, which had the same chemical structure as the PTFE supports, were not sufficiently low at approximately 60 barrer [64] to reduce the H_2 permeability of the composites. Thus, the reduction in the H_2 permeability for the composites was attributed to the decrease in the water volume fraction due to the reinforcement. The enhanced gas barrier property of the composite membranes was also supported by the results shown in Fig. 8 through the relation $i_x \sim P/t$ [65]. The low gas permeability could be effective in increasing the lifetime of PEMs by reducing the concentration of O_2, which is a reactant for the generation of active hydroxyl radicals (HO•). After the PEMWE performance test, a constant current (2 A/cm^2) was applied to monitor the degradation rate (rate of voltage increase) of the membranes, as shown in Fig. 8b and c. In the case of the most H_2-permeable SPAES60, cell failure occurred because of an electric shortage, as indicated by the abrupt voltage drop (red arrow in Fig. 8c) after 30 h. The internal short circuiting of the membrane leads the current flows without ionic current, even under a hydrogen evolution potential, resulting in a higher current density at a certain voltage compared to a membrane without an electric shortage [66]. Therefore, at a constant current density, the electric shortage is observed by the voltage drop, similar to the study of Klose et al. [63]. The electric shortage was confirmed from the polarization curves of SPAES60 before and after the durability test (Fig. S12). Hence, the degradation rate was evaluated during the initial 30 h of operation for an accurate comparison. The degradation rates of SPAES50 and SPAES60 were 323 and 1140 μV/h, respectively, and they were considerably reduced to 229 and 744 μV/h for 50/F and 60/F, respectively. After 100 h, the durability of 50/F was better than that of SPAES50 (Fig. 8b). It should be noted that there were voltage fluctuations for all the samples during the test, as shown in Fig. 8b and c, probably due to the accumulation and release of gas bubbles. The presence of gaseous products in PEMWE can alter the mass transportation and affect the overpotential even at a constant current operation [67–70]. However, the *in situ* degradation rate did not follow the trend of the H_2 permeability (Fig. S11). The membrane with lower dimensional stability (Fig. 2a and b) and higher *ex situ* chemical degradation (Fig. 5) exhibited poor durability in the *in situ* degradation profile (Fig. 8b and c). This strongly indicated that the chemically weighted PEM durability was affected by the chemical and mechanical stability of the membranes.

4. Conclusions

Hydrocarbon-based SPAES ionomers were constrained by PTFE networks to enhance the dimensional stability of highly swellable SPAES ionomers. The constrained ionomers imbibed less water compared to the freely swollen ionomers because of the mechanical resistance of the PTFE networks. Newman's membrane model and the experimental

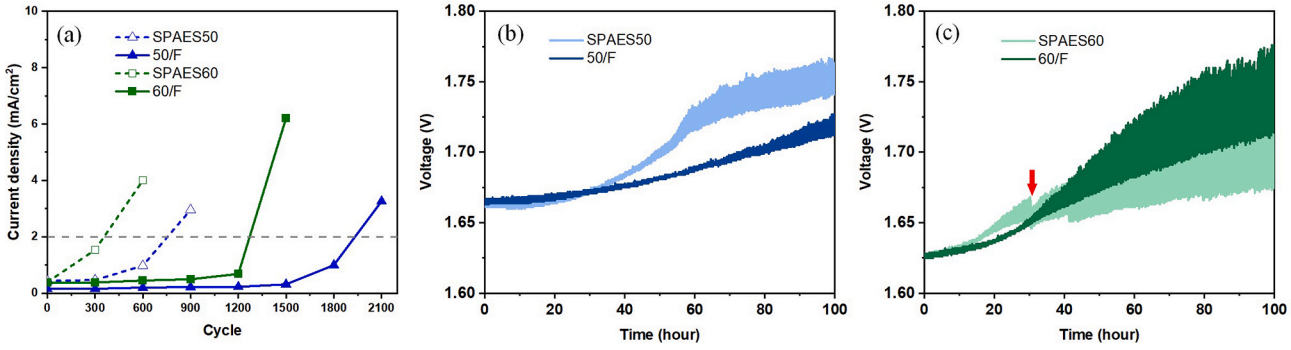

Fig. 8. a) Current density induced by H_2 crossover (i_x) of the membranes during the wet and dry cycling test at 80 °C. Transient voltage profile at a constant current density of 2 A/cm^2 in PEMWE single cells with (b) SPAES50/50/F and (c) SPAES60/60/F membranes at 80 °C for 100 h. The red arrow indicates the point cell failure due to an electrical shortage. (For interpretation of the references to colour in this figure legend, the reader is referred to the Web version of this article.)

water uptake values were used to show that the reinforcement through PTFE supports provided a stress of approximately 28 MPa, which was equivalent to the external mechanical stress required for preventing the swelling of the ionomers. This synergistically enhanced the chemical and mechanical durability of the ionomers in moisture involved PEMFCs and PEMWEs. Specifically, the dimensional stability, mechanical toughness, and oxidative resistance were noticeably improved in liquid water after the infiltration of the SPAES ionomers into the PTFE supports. These enhanced mechanochemical stabilities increased the durability of PEMFCs by 3−4-fold during wet–dry cycles and decreased the degradation rate of PEMWEs by approximately 1.5 times during long-term operation.

CRediT authorship contribution statement

Seung Jae Hong: Investigation, Formal analysis, Writing - original draft. **Hwan Yeop Jung:** Investigation, Formal analysis, Writing – original draft. **Sang Jun Yoon:** Methodology, Investigation. **Keun-Hwan Oh:** Methodology, Investigation. **Seong-Geun Oh:** Methodology, Investigation. **Young Taik Hong:** Methodology, Investigation. **Duk Man Yu:** Conceptualization, Supervision, Investigation, Writing - original draft. **Soonyong So:** Conceptualization, Investigation, Writing – original draft, Supervision.

Declaration of competing interest

The authors declare that they have no known competing financial interests or personal relationships that could have appeared to influence the work reported in this paper.

Data availability

Data will be made available on request.

Acknowledgments

This work is supported by the KRICT Core Research Program (KK2022-20), and the Hydrogen Energy Innovation Technology Development Program of the National Research Foundation of Korea (NRF) funded by the Korean government (Ministry of Science and ICT (MSIT)), NRF-2019M3E6A1064729, and also by the National R&D Program through the NRF funded by MSIT (NRF-2021M3H4A6A02045221).

Appendix A. Supplementary data

Supplementary data to this article can be found online at https://doi.org/10.1016/j.jpowsour.2022.232221.

References

[1] S. Bose, T. Kuila, T.X.H. Nguyen, N.H. Kim, K.T. Lau, J.H. Lee, Polymer membranes for high temperature proton exchange membrane fuel cell: recent advances and challenges, Prog. Polym. Sci. 36 (2011) 813–843, https://doi.org/10.1016/j.progpolymsci.2011.01.003.

[2] A. Rajput, P.P. Sharma, V. Yadav, V. Kulshrestha, Highly stable graphene oxide composite proton exchange membrane for electro-chemical energy application, Int. J. Hydrogen Energy 45 (2020) 16976–16983, https://doi.org/10.1016/j.ijhydene.2019.06.108.

[3] L. Ma, S. Sui, Y. Zhai, Investigations on high performance proton exchange membrane water electrolyzer, Int. J. Hydrogen Energy 34 (2009) 678–684, https://doi.org/10.1016/j.ijhydene.2008.11.022.

[4] F. Liu, S. Wang, D. Wang, G. Liu, Y. Cui, D. Liang, X. Wang, Z. Yong, Z. Wang, Multifunctional poly(ionic liquid)s cross-linked polybenzimidazole membrane with excellent long-term stability for high temperature-proton exchange membranes fuel cells, J. Power Sources 494 (2021), 229732, https://doi.org/10.1016/j.jpowsour.2021.229732.

[5] J. Escorihuela, R. Narducci, V. Compañ, F. Costantino, Proton conductivity of composite polyelectrolyte membranes with metal-organic frameworks for fuel cell applications, Adv. Mater. Interfac. 6 (2019), 1801146, https://doi.org/10.1002/admi.201801146.

[6] C. Yin, J. Li, Y. Zhou, H. Zhang, P. Fang, C. He, Phase separation and development of proton transport pathways in metal oxide nanoparticle/nafion composite membranes during water uptake, J. Phys. Chem. C 122 (2018) 9710–9717, https://doi.org/10.1021/acs.jpcc.8b02535.

[7] A. Kusoglu, A.Z. Weber, New insights into perfluorinated sulfonic-acid ionomers, Chem. Rev. 117 (2017) 987–1104, https://doi.org/10.1021/acs.chemrev.6b00159.

[8] L. Liu, W. Chen, Y. Li, An overview of the proton conductivity of nafion membranes through a statistical analysis, J. Membr. Sci. 504 (2016) 1–9, https://doi.org/10.1016/j.memsci.2015.12.065.

[9] M. Mukaddam, E. Litwiller, I. Pinnau, Gas sorption, diffusion, and permeation in nafion, Macromolecules 49 (2016) 280–286, https://doi.org/10.1021/acs.macromol.5b02578.

[10] K. Sopian, W.R. Wan Daud, Challenges and future developments in proton exchange membrane fuel cells, Renew. Energy 31 (2006) 719–727, https://doi.org/10.1016/j.renene.2005.09.003.

[11] Y. Shao, G. Yin, Z. Wang, Y. Gao, Proton exchange membrane fuel cell from low temperature to high temperature: material challenges, J. Power Sources 167 (2007) 235–242, https://doi.org/10.1016/j.jpowsour.2007.02.065.

[12] W. Dai, Y. Shen, Z. Li, L. Yu, J. Xi, X. Qiu, SPEEK/Graphene oxide nanocomposite membranes with superior cyclability for highly efficient vanadium redox flow battery, J. Mater. Chem. A. 2 (2014) 12423–12432, https://doi.org/10.1039/c4ta02124j.

[13] K.H. Lee, J.Y. Chu, A.R. Kim, D.J. Yoo, Enhanced performance of a sulfonated poly (arylene ether ketone) block copolymer bearing pendant sulfonic acid groups for polymer electrolyte membrane fuel cells operating at 80% relative humidity, ACS Appl. Mater. Interfaces 10 (2018) 20835–20844, https://doi.org/10.1021/acsami.8b03790.

[14] C. Wang, B. Shen, C. Xu, X. Zhao, J. Li, Side-chain-type poly(arylene ether sulfone)s containing multiple quaternary ammonium groups as anion exchange membranes, J. Membr. Sci. (2015), https://doi.org/10.1016/j.memsci.2015.05.060.

[15] B. Wang, L. Hong, Y. Li, L. Zhao, C. Zhao, H. Na, Property enhancement effects of side-chain-type naphthalene-based sulfonated poly(arylene ether ketone) on nafion composite membranes for direct methanol fuel cells, ACS Appl. Mater. Interfaces 9 (2017) 32227–32236, https://doi.org/10.1021/acsami.7b08566.

[16] P. Wen, Z. Zhong, L. Li, F. Shen, X.D. Li, M.H. Lee, A novel approach to prepare photocrosslinked sulfonated poly(arylene ether sulfone) for proton exchange membrane, J. Membr. Sci. 463 (2014) 58–64, https://doi.org/10.1016/j.memsci.2014.03.042.

[17] S.R. Choi, D.Y. Kim, W.Y. An, S. Choi, K. Park, S.D. Yim, J.Y. Park, Assessing the degradation pattern and mechanism of membranes in polymer electrolyte membrane fuel cells using open-circuit voltage hold and humidity cycle test protocols, Mater. Sci. Energy Technol. 5 (2022) 66–73, https://doi.org/10.1016/j.mset.2021.12.001.

[18] Y. Qin, S. Ma, Y. Chang, Y. Liu, Y. Yin, J. Zhang, Z. Liu, K. Jiao, Q. Du, Modeling the membrane/CL delamination with the existence of CL crack under RH cycling conditions of PEM fuel cell, Int. J. Hydrogen Energy 46 (2021) 8722–8735, https://doi.org/10.1016/j.ijhydene.2020.12.043.

[19] S.-Y. Han, D.M. Yu, Y.-H. Mo, S.M. Ahn, J.Y. Lee, T.-H. Kim, S.J. Yoon, S. Hong, Y. T. Hong, S. So, Ion exchange capacity controlled biphenol-based sulfonated poly (arylene ether sulfone) for polymer electrolyte membrane water electrolyzers: comparison of random and multi-block copolymers, J. Membr. Sci. 634 (2021), 119370, https://doi.org/10.1016/j.memsci.2021.119370.

[20] S. Garbe, J. Futter, T.J. Schmidt, L. Gubler, Insight into elevated temperature and thin membrane application for high efficiency in polymer electrolyte water electrolysis, Electrochim. Acta 377 (2021), 138046, https://doi.org/10.1016/j.electacta.2021.138046.

[21] D. Wang, C.J. Cornelius, Modeling ionomer swelling dynamics of a sulfonated polyphenylene, pentablock copolymers, and nafion, J. Polym. Sci., Part B: Polym. Phys. 55 (2017) 435–443, https://doi.org/10.1002/polb.24284.

[22] C.J. Lee, J. Song, K.S. Yoon, Y. Rho, D.M. Yu, K.H. Oh, J.Y. Lee, T.H. Kim, Y. T. Hong, H.J. Kim, S.J. Yoon, S. So, Controlling hydrophilic channel alignment of perfluorinated sulfonic acid membranes via biaxial drawing for high performance and durable polymer electrolyte membrane water electrolysis, J. Power Sources 518 (2022), 230772, https://doi.org/10.1016/j.jpowsour.2021.230772.

[23] T.Y. Son, T.H. Kim, S.Y. Nam, Crosslinked pore-filling anion exchange membrane using the cylindrical centrifugal force for anion exchange membrane fuel cell system, Polymers 12 (2020) 1–15, https://doi.org/10.3390/polym12112758.

[24] H. Jung, K. Fujii, T. Tamaki, H. Ohashi, T. Ito, T. Yamaguchi, Low fuel crossover anion exchange pore-filling membrane for solid-state alkaline fuel cells, J. Membr. Sci. 373 (2011) 107–111, https://doi.org/10.1016/j.memsci.2011.02.044.

[25] V. Vijayakumar, T.Y. Son, S.Y. Nam, Recent advances in composite polymer electrolyte membranes for fuel cell, Appl. Chem. Eng. 30 (2019) 1–10, https://doi.org/10.14478/ace.2018.1105.

[26] C. Zhang, X. Yue, Y. Mu, X. Zuo, N. Lu, Y. Luo, R. Na, S. Zhang, G. Wang, Novel pore-filling membrane based on block sulfonated poly (ether sulphone) with enhanced proton conductivity and methanol resistance for direct methanol fuel cells, Electrochim. Acta 307 (2019) 188–196, https://doi.org/10.1016/j.electacta.2019.03.189.

[27] S. Feng, Z. Zhong, Y. Wang, W. Xing, E. Drioli, Progress and perspectives in PTFE membrane: preparation, modification, and applications, J. Membr. Sci. 549 (2018) 332–349, https://doi.org/10.1016/j.memsci.2017.12.032.

[28] T.Y. Son, T.H. Kim, S.Y. Nam, Crosslinked pore-filling anion exchange membrane using the cylindrical centrifugal force for anion exchange membrane fuel cell system, Polymers 12 (2020) 1–15, https://doi.org/10.3390/polym12112758.

[29] H. Jung, K. Fujii, T. Tamaki, H. Ohashi, T. Ito, T. Yamaguchi, Low fuel crossover anion exchange pore-filling membrane for solid-state alkaline fuel cells, J. Membr. Sci. 373 (2011) 107–111, https://doi.org/10.1016/j.memsci.2011.02.044.
[30] V. Vijayakumar, T.Y. Son, S.Y. Nam, Recent advances in composite polymer electrolyte membranes for fuel cell, Appl. Chem. Eng. 30 (2019) 1–10, https://doi.org/10.14478/ace.2018.1105.
[31] C. Zhang, X. Yue, Y. Mu, X. Zuo, N. Lu, Y. Luo, R. Na, S. Zhang, G. Wang, Novel pore-filling membrane based on block sulfonated poly (ether sulphone) with enhanced proton conductivity and methanol resistance for direct methanol fuel cells, Electrochim. Acta 307 (2019) 188–196, https://doi.org/10.1016/j.electacta.2019.03.189.
[32] S. Feng, Z. Zhong, Y. Wang, W. Xing, E. Drioli, Progress and perspectives in PTFE membrane: preparation, modification, and applications, J. Membr. Sci. 549 (2018) 332–349, https://doi.org/10.1016/j.memsci.2017.12.032.
[33] J. Miyake, M. Kusakabe, A. Tsutsumida, K. Miyatake, Remarkable reinforcement effect in sulfonated aromatic polymers as fuel cell membrane, ACS Appl. Energy Mater. 1 (2018) 1233–1238, https://doi.org/10.1021/acsaem.7b00349.
[34] L. Yu, F. Lin, L. Xu, J. Xi, Structure-property relationship study of Nafion XL membrane for high-rate, long-lifespan, and all-climate vanadium flow batteries, RSC Adv. 7 (2017) 31164–31172, https://doi.org/10.1039/C7RA04996J.
[35] Y. Garsany, R.W. Atkinson, M.B. Sassin, R.M.E. Hjelm, B.D. Gould, K.E. Swider-Lyons, Improving PEMFC performance using short-side-chain low-equivalent-weight PFSA ionomer in the cathode catalyst layer, J. Electrochem. Soc. 165 (2018) F381–F391, https://doi.org/10.1149/2.1361805jes.
[36] S. Shi, X. Sun, Q. Lin, J. Chen, Y. Fu, X. Hong, C. Li, X. Guo, G. Chen, X. Chen, Fatigue crack propagation behavior of fuel cell membranes after chemical degradation, Int. J. Hydrogen Energy 45 (2020) 27653–27664, https://doi.org/10.1016/j.ijhydene.2020.07.113.
[37] R. Gloukhovski, V. Freger, Y. Tsur, Understanding methods of preparation and characterization of pore-filling polymer composites for proton exchange membranes: a beginner's guide, Rev. Chem. Eng. 34 (2018) 455–479, https://doi.org/10.1515/revce-2016-0065.
[38] T. Yamaguchi, F. Miyata, S.I. Nakao, Pore-filling type polymer electrolyte membranes for a direct methanol fuel cell, J. Membr. Sci. 214 (2003) 283–292, https://doi.org/10.1016/S0376-7388(02)00579-3.
[39] J. Miyake, T. Watanabe, H. Shintani, Y. Sugawara, M. Uchida, K. Miyatake, Reinforced polyphenylene ionomer membranes exhibiting high fuel cell performance and mechanical durability, ACS Mater. Au. 1 (2021) 81–88, https://doi.org/10.1021/acsmaterialsau.1c00002.
[40] K. Kim, S.K. Kim, J.O. Park, S.W. Choi, K.H. Kim, T. Ko, C. Pak, J.C. Lee, Highly reinforced pore-filling membranes based on sulfonated poly(arylene ether sulfone) s for high-temperature/low-humidity polymer electrolyte membrane fuel cells, J. Membr. Sci. 537 (2017) 11–21, https://doi.org/10.1016/j.memsci.2017.05.014.
[41] A.Z. Weber, J. Newman, A theoretical study of membrane constraint in polymer-electrolyte fuel cells, AIChE J. 50 (2004) 3215–3226, https://doi.org/10.1002/aic.10230.
[42] K.B. Wiles, F. Wang, J.E. McCrath, Directly copolymerized poly(arylene sulfide sulfone) disulfonated copolymers for PEM-based fuel cell systems. I. Synthesis and characterization, J. Polym. Sci. Part A Polym. Chem. 43 (2005) 2964–2976, https://doi.org/10.1002/pola.20744.
[43] Appendix A: FCTT AST and polarization curve protocols for PEMFC s. https://www.energy.gov/sites/default/files/2015/08/f25/fcto_dwg_usdrive_fctt_accelerated_stress_tests_jan2013.pdf.
[44] S.J. Hong, S.J. Yoon, T.-H. Kim, J.Y. Lee, S.-G. Oh, Y.T. Hong, S. So, D.M. Yu, Alcohol-treated porous PTFE substrate for the penetration of PTFE-incompatible hydrocarbon-based ionomer solutions, Langmuir. 0 (n.d.) null-null. doi:10.1021/acs.langmuir.1c00120.
[45] Y.S. Kim, M.A. Hickner, L. Dong, B.S. Pivovar, J.E. McGrath, Sulfonated poly (arylene ether sulfone) copolymer proton exchange membranes: composition and morphology effects on the methanol permeability, J. Membr. Sci. 243 (2004) 317–326, https://doi.org/10.1016/j.memsci.2004.06.035.
[46] C. Ajith, A.P. Deshpande, S. Varughese, Proton conductivity in crosslinked hydrophilic ionic polymer system: competitive hydration, crosslink heterogeneity, and ineffective domains, J. Polym. Sci., Part B: Polym. Phys. 54 (2016) 1087–1101, https://doi.org/10.1002/polb.24012.
[47] A.Z. Weber, J. Newman, Transport in polymer-electrolyte membranes, J. Electrochem. Soc. 151 (2004) A326, https://doi.org/10.1149/1.1639158.
[48] P. Goyal, C.W. Monroe, New foundations of Newman's theory for solid electrolytes: thermodynamics and transient balances, J. Electrochem. Soc. 164 (2017) E3647–E3660, https://doi.org/10.1149/2.0611711jes.
[49] G. Calleja, A. Jourdan, B. Ameduri, J.P. Habas, Where is the glass transition temperature of poly(tetrafluoroethylene)? A new approach by dynamic rheometry and mechanical tests, Eur. Polym. J. 49 (2013) 2214–2222, https://doi.org/10.1016/j.eurpolymj.2013.04.028.
[50] S. Shi, A.Z. Weber, A. Kusoglu, Structure/property relationship of Nafion XL composite membranes, J. Membr. Sci. 516 (2016) 123–134, https://doi.org/10.1016/j.memsci.2016.06.004.
[51] L. Liu, Y. Li, R. Qiao, Y. Xing, H. Li, Reinforced composite membranes based on expanded polytetrafluoroethylene skeletons modified by a surface sol-gel process for fuel cell applications, Energy Fuel. 35 (2021) 12482–12494, https://doi.org/10.1021/acs.energyfuels.1c01205.
[52] S.S. Rangaraj, S.B. Bhaduri, A modified rule-of-mixtures for prediction of tensile strengths of unidirectional fibre-reinforced composite materials, J. Mater. Sci. 29 (1994) 2795–2800, https://doi.org/10.1007/BF00356835.
[53] Q. Feng, X.Z. Yuan, G. Liu, B. Wei, Z. Zhang, H. Li, H. Wang, A review of proton exchange membrane water electrolysis on degradation mechanisms and mitigation strategies, J. Power Sources 366 (2017) 33–55, https://doi.org/10.1016/j.jpowsour.2017.09.006.
[54] J. Lawrence, T. Yamaguchi, The degradation mechanism of sulfonated poly (arylene ether sulfone)s in an oxidative environment, J. Membr. Sci. 325 (2008) 633–640, https://doi.org/10.1016/j.memsci.2008.08.027.
[55] M. Chandesris, V. Médeau, N. Guillet, S. Chelghoum, D. Thoby, F. Fouda-Onana, Membrane degradation in PEM water electrolyzer: numerical modeling and experimental evidence of the influence of temperature and current density, Int. J. Hydrogen Energy 40 (2015) 1353–1366, https://doi.org/10.1016/j.ijhydene.2014.11.111.
[56] T. Mochizuki, R. Shimizu, K. Miyatake, R. Akiyama, M. Uchida, R. Taki, J. Miyake, Design of flexible polyphenylene proton-conducting membrane for next-generation fuel cells, Sci. Adv. 3 (2017), eaao0476, https://doi.org/10.1126/sciadv.aao0476.
[57] T. Tanaka, H. Shintani, Y. Sugawara, A. Masuda, N. Sato, M. Uchida, K. Miyatake, Wet/dry cycle durability of polyphenylene ionomer membranes in PEFC, J. Power Sources Adv. 10 (2021), 100063, https://doi.org/10.1016/j.powera.2021.100063.
[58] K. Shiino, T. Otomo, T. Yamada, H. Arima, K. Hiroi, S. Takata, J. Miyake, K. Miyatake, Structural investigation of sulfonated polyphenylene ionomers for the design of better performing proton-conductive membranes, ACS Appl. Polym. Mater. 2 (2020) 5558–5565, https://doi.org/10.1021/acsapm.0c00895.
[59] M. Adamski, N. Peressin, S. Holdcroft, On the evolution of sulfonated polyphenylenes as proton exchange membranes for fuel cells, Mater, Advisor 2 (2021) 4966–5005, https://doi.org/10.1039/d1ma00511a.
[60] T. Tanaka, H. Shintani, Y. Sugawara, A. Masuda, N. Sato, M. Uchida, K. Miyatake, Wet/dry cycle durability of polyphenylene ionomer membranes in PEFC, J. Power Sources Adv. 10 (2021), 100063, https://doi.org/10.1016/j.powera.2021.100063.
[61] R. Omrani, B. Shabani, Hydrogen crossover in proton exchange membrane electrolysers: the effect of current density, pressure, temperature, and compression, Electrochim. Acta 377 (2021), 138085, https://doi.org/10.1016/j.electacta.2021.138085.
[62] A. Daryaei, G.C. Miller, J. Willey, S.R. Choudhury, B. Vondrasek, D. Kazerooni, M. R. Burtner, C. Mittelsteadt, J.J. Lesko, J.S. Ri, J.E. Mcgrath, Synthesis and membrane properties of sulfonated poly (arylene ether sulfone) statistical copolymers for electrolysis of water : influence of meta- and para-substituted comonomers, ACS Appl. Mater. Interfaces 9 (2017) 20067–20075, https://doi.org/10.1021/acsami.7b02401.
[63] C. Klose, T. Saatkamp, A. Münchinger, L. Bohn, G. Titvinidze, M. Breitwieser, K. Kreuer, S. Vierrath, All-hydrocarbon MEA for PEM water electrolysis combining low hydrogen crossover and high efficiency, Adv. Energy Mater. 10 (2020), 1903995, https://doi.org/10.1002/aenm.201903995.
[64] Z. Qiao, Z. Wang, C. Zhang, S. Yuan, Y. Zhu, J. Wang, Characterization of gas crossover and its implications in PEM fuel cells, AIChE J. 59 (2006) 215–228, https://doi.org/10.1002/aic.
[65] B. Bensmann, R. Hanke-Rauschenbach, K. Sundmacher, In-situ measurement of hydrogen crossover in polymer electrolyte membrane water electrolysis, Int. J. Hydrogen Energy 39 (2014) 49–53, https://doi.org/10.1016/j.ijhydene.2013.10.085.
[66] S.P.S. Badwal, S. Giddey, F.T. Ciacchi, Hydrogen and oxygen generation with polymer electrolyte membrane (PEM)-based electrolytic technology, Ionics 12 (2006) 7–14, https://doi.org/10.1007/s11581-006-0002-x.
[67] K.J. Choi, H. Kim, S.K. Kim, Multicomponent nonprecious hydrogen evolution catalysts for high performance and durable proton exchange membrane water electrolyzer, J. Power Sources 506 (2021), 230200, https://doi.org/10.1016/j.jpowsour.2021.230200.
[68] G.H. Han, H. Kim, J. Kim, J. Kim, S.Y. Kim, S.H. Ahn, Micro-nanoporous MoO2@CoMo heterostructure catalyst for hydrogen evolution reaction, Appl. Catal. B Environ. 270 (2020), 118895, https://doi.org/10.1016/j.apcatb.2020.118895.
[69] H. Huang, L. Chen, C. Liu, X. Liu, S. Fang, W. Liu, Y. Liu, Hierarchically nanostructured MoS2 with rich in-plane edges as a high-performance electrocatalyst for the hydrogen evolution reaction, J. Mater. Chem. A. 4 (2016) 14577–14585, https://doi.org/10.1039/c6ta06174e.
[70] H. Vogt, The actual current density of gas-evolving electrodes - notes on the bubble coverage, Electrochim. Acta 78 (2012) 183–187.